Electrochimica Acta 388 (2021) 138590

Contents lists available at ScienceDirect

Electrochimica Acta

journal homepage: www.elsevier.com/locate/electacta

Changes in electrode resistances and limiting currents as a function of microbial electrolysis cell reactor configurations

Gahyun Baek, Ruggero Rossi, Bruce E. Logan*

Department of Civil and Environmental Engineering, The Pennsylvania State University, 231Q Sackett Building, University Park, PA 16802, USA

ARTICLE INFO

Article history:
Received 8 March 2021
Accepted 7 May 2021
Available online 16 May 2021

Keywords:
Electrode potential slope method
electrode size ratio
internal resistance
microbial electrolysis cell
polarization curve

ABSTRACT

Quantifying the resistances that different components of microbial electrolysis cells (MECs) contribute to the total internal resistance is important for understanding how different reactor configurations affect overall performance. The impact of the reactor architecture was examined here by varying the relative sizes of the electrodes and quantifying the changes in resistances of the electrodes and limiting current densities as a function of the applied potential (E_{ap}). The MECs with equal cathode:anode size ratios (S_R=1), showed a steady increase in current up to 1.8 mA for E_{ap}'s ≤ 0.9 V. However, lower limiting currents were obtained for configurations with smaller anodes as shown by a lack of an increase in current for E_{ap} > 0.7 V (limiting current of 0.8 mA, S_R=16, and 1.0 mA, S_R=4). The largest component of the internal resistance changed with the relative sizes of the electrodes. For example, the cathode resistance was 58% of the internal resistance for the configuration of S_R=1 and 51% for S_R=2, but the anode was 57% of the internal resistance for S_R=16. These results show how differences in reactor architectures can be quantified in terms of individual electrode resistances and limiting currents using polarization data obtained by varying the applied potentials.

1. Introduction

Microbial electrolysis cells (MECs) are being investigated as an approach to decrease energy use or even achieve net energy production from wastewater treatment. In MECs organic matter is oxidized by exoelectrogenic bacteria on the anode and the current generated is used to produce H_2 gas at the cathode [1,2]. MECs require an external power source to drive H_2 generation at the cathode as the reaction is not exothermic for useful operational conditions [3]. A voltage larger than ~0.2 V is needed in practice to be added to the voltage generated by the bacteria to produce H_2 gas [4]. The applied potential (E_{ap}) added to the circuit is usually chosen to provide a balance between using higher voltage to produce larger current densities or using lower voltages to reduce the energy consumption by the process to maximize energy recovery [5,6]. The selected E_{ap} impacts energy recovery based on $\eta = 148/E_{ap}$ (higher heating value, HHV of hydrogen), or $\eta = 123/E_{ap}$ (lower heating value, LHV) [3,7], where η (%) is the maximum percentage energy recovery based on the E_{ap} under standard conditions. For example, at E_{ap}= 0.9 V, the maximum energy recovery is 137% (HHV) based on recovery of all hydrogen gas produced in proportion to the current generated. MECs have typically been operated using only a single E_{ap} within a range of 0.2–1.5 V in previous studies [8], with the most common E_{ap}'s chosen as a single applied potential in the range of 0.6–1.0 V [9]. If only a single applied voltage is examined for an MEC then there are no polarization data (a plot of voltage as a function of current) for a more in-depth analysis of MEC performance.

The importance of obtaining polarization data to quantify the anode, cathode, solution and total internal resistances is now well recognized for microbial fuel cells (MFCs), but not for MECs due to a lack of individual electrode polarization data [10,11]. Polarization data are needed for MECs so that the main factors limiting higher current densities with applied potentials can be identified. In MFCs, polarization data are used to produce power density curves which typically are bell-shaped. However, sometimes a rapid decrease in power density is observed after the maximum power density point is reached. This decrease results in a power density curve that turns back to lower current densities when using lower external resistances in the circuit (referred to as power overshoot) because the anodes reach a limiting current and thus fails to achieve a higher current density at lower resistances [12]. The reasons for a limiting current include insufficient anode biomass, localized low pH conditions, or insufficient anode acclimation [13]. In MECs the anode can similarly limit the ability of the system to produce higher currents due to the anode reaching a limiting current [14]. However, there are few studies that re-

* Corresponding author.
E-mail address: blogan@psu.edu (B.E. Logan).

https://doi.org/10.1016/j.electacta.2021.138590
0013-4686/

Table 1
Normalized surface area the electrodes and electrode surface area ratio.

Calculation basis	C_1A_1	$C_1A_{0.5}$	$C_2A_{0.5}$	$C_4A_{0.25}$
$a_{P,A}$ of the anode (m^2 m^{-3})[a]	30	15	15	7.5
$a_{P,A}$ of the cathode (m^2 m^{-3})	30	30	60	120
S_R based on the $a_{P,A}$[b]	1	2	4	16
$a_{S,A}$ of the anode (m^2 m^{-3})[c]	92	52	52	31
$a_{S,A}$ of the cathode (m^2 m^{-3})	76	76	152	305

[a] Projected surface area normalized by liquid volume.
[b] cathode:anode size ratio.
[c] Total surface area normalized by liquid volume.

port polarization data for MECs by either varying the applied voltage (or scanning the anode potentials) over a range of E_{ap} values where limiting currents might be observed [14-18]. Routine reporting of polarization data for MECs is needed to provide a better understanding of the electrode performance in terms of their relative resistances as well as avoid the application of E_{ap}'s greater than those needed to produce high current densities.

The utility of polarization data for analyzing how the reactor architecture impacts performance in terms of electrode resistances and limiting currents was shown here by obtaining polarization data for MECs with different relative electrode sizes. Four different cathode:anode sizes were used to produce MEC configurations that had different responses to applied voltages. To calculate the electrode resistances, the applied voltage was varied to obtain polarization curves for the whole MEC, and with a reference electrode it was possible to investigate the relative contribution of the anode and cathode resistances. These data were used to calculate the electrode resistances using the electrode potential slope (EPS) method [14,19]. The overall system performance was also examined in terms of organic removal and biogas production rates. Although different reactors have been developed that have different electrode sizes [16,20,21] there has been no side-by-side evaluation of MECs with different electrode dimensions in terms of individual electrode performance through measurement of their internal resistances. The analysis of the response of these different MECs that have different electrodes sizes can show the utility of polarization data for identifying limiting anode current densities as well as quantifying the resistances of the electrodes and thus provide insight into the factors limiting performance.

2. Materials and methods

2.1. Configurations and construction of MECs

Single-chamber MECs were constructed using 5-mL serum bottles (empty volume of 8 mL; Wheaton, Millville, NJ, USA). Four different MEC configurations were prepared by varying the ratio of the cathode:anode sizes (S_R) from S_R=1 to S_R=16 based on the projected surface area of one side of each electrode (Fig. 1). The anode was a graphite plate (Grade GM-10; GraphiteStore, Buffalo Grove, IL, USA) 1.5-cm × 1-cm × 0.32-cm, yielding a projected anode area of A_1 = 1.5 cm^2, surface area of $a_{P,A}$ = 30 m^2 m^{-3} based on only the projected surface area per liquid volume (5 mL), and $a_{S,A}$ = 92 m^2 m^{-3} based on the area of all sides. The ratio of electrode sizes was controlled by reducing the anode size by cutting it in half or by increasing the cathode size (Table 1). Anodes were reduced in size by ½ to $A_{0.5}$ =0.75 cm^2, or by ¼ to $A_{0.25}$ =0.375 cm^2. Stainless steel (SS) mesh (Type 304, mesh size 60 × 60; McMaster-Carr) was used as the cathode, with a mesh size of 1.5-cm × 1-cm designed as C_1 = 1.5 cm^2 as it was the same size as the largest anode. Cathode sizes were increased to provide larger projected surface areas, with cathodes twice (C_2 = 3 cm^2) or four times (C_4 = 6 cm^2) as large as the smallest cathode. The largest cathode was partially bent into a hemisphere shape to fit through the bottle neck, and then it extended partly around the anode compared to the other more parallel orientations of the different electrode configurations (Fig. 1C). MECs with equally sized electrodes, or S_R=1, were designated as C_1A_1 with ratios for the other reactors of $C_1A_{0.5}$ (S_R=2) and $C_2A_{0.5}$ (S_R=4), and $C_4A_{0.25}$ (S_R=16). For reactors $C_4A_{0.25}$, a double layer of SS mesh (two pieces of 1.5-cm × 2-cm mesh) was used due to the limited space in the reactor.

Anodes were polished using sandpaper, sonicated in acetone for 20 min, immersed in 1 N HCl overnight, and rinsed three times with deionized water before use to remove any contaminants. Anodes were connected using titanium wires (0.08 cm diameter; McMaster-Carr) and the cathodes were connected using SS wire (0.10 cm diameter; Malin Co.). Only anodes or cathodes with a contact resistance <1.0 Ω were used in tests. Reactors were sealed with a thick butyl rubber stopper and aluminum caps to maintain anaerobic conditions (Fig. 1). The rigid titanium and SS wires holding the electrodes were pierced though the rubber stopper to maintain the electrode spacing to be *ca.* 1 cm.

2.2. Reactor operation

MECs were inoculated with 50% (v/v) of fresh medium and effluent from MECs fed a medium containing 1 g L^{-1} of sodium acetate. The MEC inoculum was omitted from the third batch cycle and the MECs were subsequently fed only fresh medium. The MECs were operated in fed-batch mode with 50 mM phosphate buffer solution (PBS), containing 2.45 g L^{-1} NaH_2PO_4•H_2O, 4.58 g L^{-1} Na_2HPO_4, 0.31 g L^{-1} NH_4Cl, 0.13 g L^{-1} KCl, mineral (12.5 mL L^{-1}) and vitamin (5 mL L^{-1}) solutions (pH =7.1, conductivity = 7.4 mS cm^{-1}), with sodium acetate (1 g L^{-1}) as the sole organic source. For each cycle, MECs were filled with fresh medium and sparged with ultra-pure nitrogen gas for 3 min.

All analyses reported here were conducted after at least 3 successive similar current production profiles were observed (Fig. S1). Experiments were conducted in triplicate in the dark without shaking in a constant temperature room (30°C). A fixed external voltage of 0.9 V was applied to MEC reactors, except as noted, using a potentiostat (VMP3, BioLogic, Knoxville, TN).

2.3. Analyses and calculations

Soluble chemical oxygen demand (SCOD) was analyzed using standard methods (TNTplus COD reagent; HACH company) with the samples filtered by a syringe filtration (0.45 μm pore diameter). Gas composition was analyzed at the end of the batch cycle using a gas chromatograph (GC, SRI Instrument, Torrance, CA, USA) for a 250 μL sample from the headspace obtained with an airtight syringe (Hamilton, Reno, NV, USA). The gas sample was collected by piercing the needle through the rubber stopper, and total gas volume based on reading the volume in the syringe was recorded at the end of each cycle. All SCOD and gas measurements were performed in duplicate.

The hydrogen or methane production (V_X) was calculated using $V_X = (V_h + V_p) f_X$, where V_h is a headspace volume, V_p is the amount of total gas production, and f_X is a fraction of hydrogen or methane in the total gas. The theoretical hydrogen or methane production (V_{th}) was calculated using $V_{th} = C_t\ V_m/nF$, where C_t is the total coulombs calculated by integrating the current over time using only the first 90% of coulombs that were obtained [7], V_m is the molar gas volume (24.2 L mol^{-1}), n is the moles of hydrogen (2) or methane (8) equivalent to one mole of electrons, and F is Faraday's constant (96,500 C mol^{-1}). The cathodic hydrogen or methane recovery (γ_{CAT}) was calculated using $\gamma_{CAT} = V_X/V_{th}$. Coulombic efficiency (CE) was calculated as CE = C_t/C_c, where C_c is the total charge consumed based on the acetate removal. To

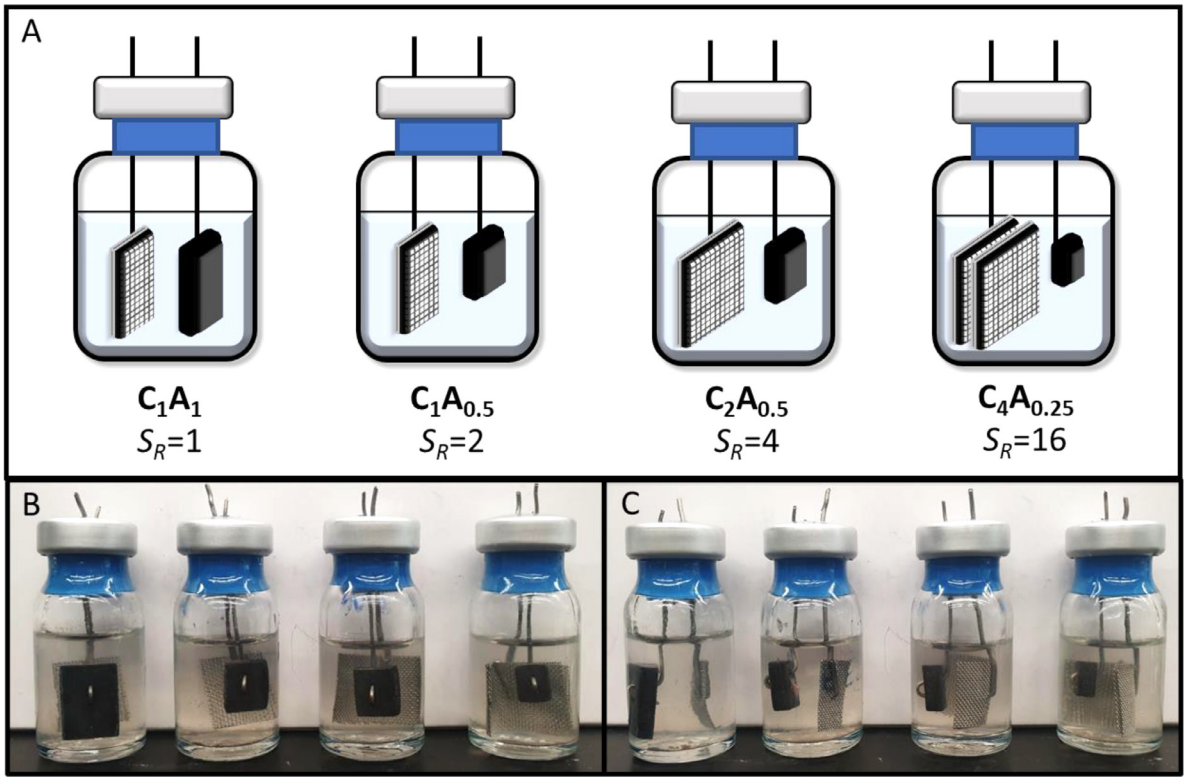

Fig. 1. (A) Schematic drawings and (B and C) photographs of the MEC configurations with varying electrode size ratio. Graphite blocks (solid black) were used as anodes and stainless steel mesh was used for the cathodes.

convert the acetate concentrations to coulombs, conversion factors were 8 mols of e^- per 1 mol of acetate and 1.07 g COD per 1 g acetate. The current density was normalized by the liquid working volume (volumetric current density; I_V) or the anode total surface area (current density per area; I_A). The maximum current density for each condition was obtained by averaging the 10 highest current densities during each cycle [22]. The energy efficiency (η_E) was calculated using $n_E = (n_{H2}\Delta H_{H2} + n_{CH4}\Delta H_{CH4})/n_E = (n_{H2}\Delta H_{H2} + n_{CH4}\Delta H_{CH4})/W_E$, where ΔH is the energy content of hydrogen (286 kJ mol^{-1}) or methane (889 kJ mol^{-1}) and W_E is the amount of energy added to the circuit using the potentiostat [16].

2.4. Electrochemical measurements

A single-cycle polarization test was performed by reducing the E_{ap} from 0.9 V to 0.3 V at 0.1 V intervals. Before the test, the reactors were fed with fresh medium and maintained at E_{ap} = 0.9 V until the current was stable (>3 h). Each voltage was lasted for 30 min and the last five points at each applied voltage were averaged to draw the polarization curve. The current was recorded every 30 s during tests. The linear portions of whole cell, anodic and cathodic potentials were used to calculate the internal resistance using the EPS method [14]. The linear portion was fitted by $E = mi + b$, where i is the current (mA), the slope m is defined as the internal resistance of each electrode (Ω), and the y-intercept was the experimental open circuit potential (mV) of each electrode. While fixed voltage (E_{cell}) was applied between electrodes, the cathode potential (E_{cat}) was measured against the reference electrode (Ag/AgCl; model RE-5B, BASi; 0.209 V vs. standard hydrogen electrode, SHE). The anode potential (E_{an}) was then calculated as $E_{an} = E_{cat} - E_{cell}$. E_{an} and E_{cat} were corrected using the solution conductivity and the distance between each electrode and the reference electrode as described previously [23,24].

Electrochemical impedance spectroscopy (EIS) was used to measure the solution resistance between each set of electrodes (i.e., anode and cathode, reference electrode and anode, or reference electrode and cathode; Fig. S3A). The MECs were set with an open circuit for 30 s and then EIS tests were conducted over a frequency range of 100 kHz to 500 Hz or 500 kHz to 500 Hz. A sinusoidal perturbation of 5 mV amplitude was applied with 10 points per decade. The impedance data were obtained based on the Nyquist plots analyzed with Zfit provided from the EC-lab software (VM3, BioLogic, Knoxville, TN) [19].

3. Results & discussions

3.1. Current generation over a fed-batch cycle

The maximum volumetric current densities over a fed-batch cycle (E_{ap} = 0.9 V) decreased with anode size, with the MEC with the largest anode (C_1A_1) producing the highest current density of 380 ± 13 A m^{-3} (Fig. 2A). The two MECs with the half-sized anodes produced about the same current densities of 249 ± 20 A m^{-3} ($C_1A_{0.5}$) and 244 ± 31 A m^{-3} ($C_2A_{0.5}$), with the MEC with the smallest anode ($C_4A_{0.25}$) producing the lowest current density of 179 ± 7 A m^{-3}. As the anode size decreased, the current density of the MEC did not substantially change until the anode was only $1/16^{th}$ the size of the cathode ($C_4A_{0.25}$) (Fig. 2B). This observation indicated that the current output did not decrease linearly with the anode size, resulting in the increased anode current density as S_R increased. This result is consistent with previous reports using MFCs where the cathode contributes more to limiting current and power generation than the anode [25,26].

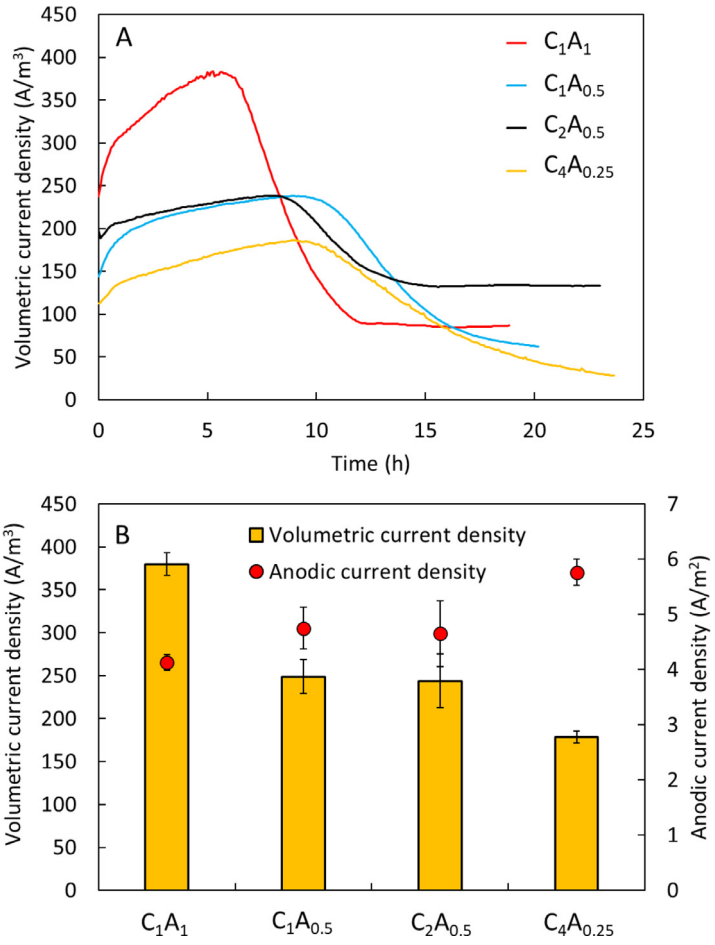

Fig. 2. (A) Volumetric current density profiles for a single representative cycle, and (B) maximum current densities calculated for a cycle. Total anode surface area ($a_{S,C}$) was used to calculate anodic current density.

3.2. Polarization tests

When polarization tests were performed by changing the applied potential from E_{ap} = 0.9 to 0.3 V, a linear response was observed with the MEC with equally sized electrodes (C_1A_1) (Fig. 3 and Fig. S2). However, for the other three MECs there was a linear increase in the current with E_{ap} only at the lower applied voltages, with a negligible increase in current at the higher applied voltages. For the two MECs with the half-sized anode ($C_1A_{0.5}$ and $C_2A_{0.5}$), the current reached a maximum of ~1 mA and then did not further increase at higher applied voltages. We define here this non-linear region, with no further appreciable increase in current, as the limiting current I_{Lim}. For the smallest anode, the limiting current was approximately I_{Lim} = 0.8 mA. In contrast to the behavior of the anodes, the current increases for the cathode were generally linear over the E_{ap} except for the C_1A_1 reactor, where there was slightly reduced performance as shown by a change in slope, rather than a limiting current (Fig. 3C). This change in slope was attributed to a shift in cathode performance due to the much higher current production for this reactor when current was not limited by the anode due to the largest size. Polarization data for both the anodes and cathodes were also linear at the lowest currents, suggesting minimal activation losses [27]. Activation losses are usually not noticeable for anodes in MECs, but such losses are more obvious for the oxygen reduction reaction in MFCs [10,28].

When the current production was normalized by total surface area of the anode, the reasons for the different behavior of the MECs with the same E_{ap} was clearer relative to anode performance (Fig. 3B). The MECs with equally sized electrodes (C_1A_1) at an E_{ap} = 0.9 V did not reach a current density that was in the region for the other MECs that produced limiting current densities. The highest current density for the C_1A_1 reactors was ~3.9 A m^{-2} with E_{ap}=0.9 V, while the two MECs with the half-sized anodes reached that same current density at E_{ap} = 0.7 V. Thus, when E_{ap} larger than 0.7 V were applied, the anodes were unable to produce a higher current as they had reached their limiting current density of ~3.9 A m^{-2}. For the smallest anode with the doubled cathode ($C_4A_{0.25}$), a slightly higher limiting current density of I_{Lim} = 5.1 ± 0.1 A m^{-2} was achieved, likely due to the use of two cathode layers that may have helped to better balance the pH around the anode surface. The acidification of the anode biofilm due to the limited proton transport out of the anode has been reported to limit current density in MFC studies [29]. Cathodes analyzed on current normalized by area showed a response similar to that based on total volumetric current (Fig. 3D), with all linear responses to applied voltages, showing most of the differences in performance among the four different MEC configurations were due to the anodes.

The occurrence of a limiting current density has not been well recognized for MECs, although this phenomenon is similar to power overshoot often observed in MFCs [30-32]. In an MFC when the external resistance is lowered past the point where the anode is unable to produce higher currents, the anode potentials increase but current does not [12,33]. This lack of an increase in current production by the anode results in a doubling back of the power density curve, and therefore power overshoot [12,33]. For MECs, rather than a lower resistance driving the anode to a maximum current density it is the applied potential which results in a maximum or limiting current density. A consequence of this limiting

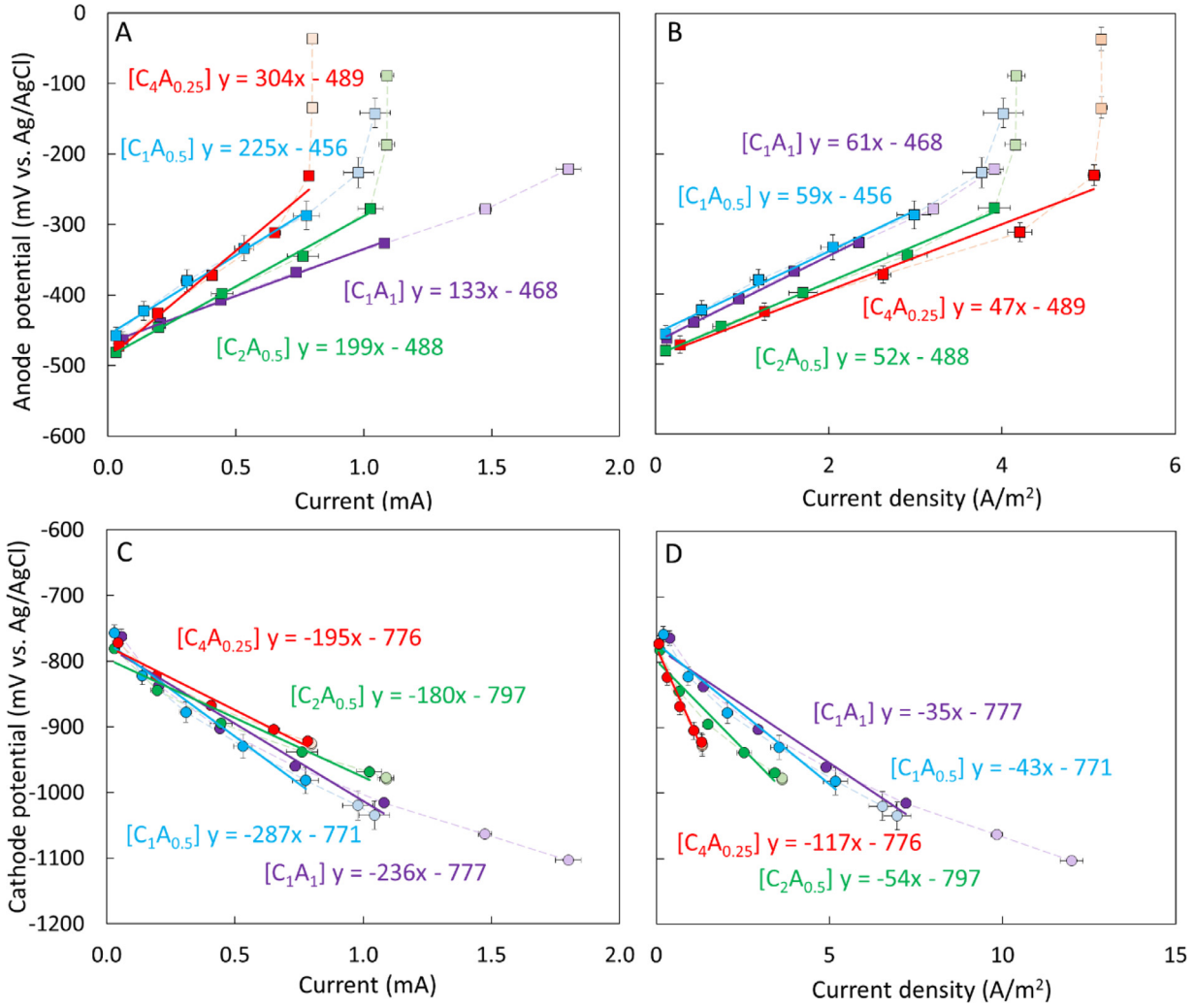

Fig. 3. Polarization data obtained by applying voltages from 0.9 to 0.3 V, with linear regressions for based on the indicated range (faded points are shown for data not included in the regression). Data shown for the anode based on (A) current, or (B) current density and for the cathode based on (C) current or (D) current density based on the total surface area ($a_{S,C}$) of the electrodes.

current density in an MEC is that energy is wasted by applying potentials above those that will increase current due to the limit in current densities by the anode.

3.3. Comparison of electrode resistances using the electrode potential slope method

The individual internal resistance of the anode and the cathode were calculated using the EPS method for current produced at lower E_{ap} using the polarization data that showed a linear response between current and E_{ap} (Fig. 4). For the MECs with larger anodes, the cathodes were the largest component of the internal resistance with 58% of the internal resistance for the C_1A_1 configuration, and 51% for the half size anode with the smaller cathode ($C_1A_{0.5}$). However, for the largest cathode ($C_4A_{0.25}$) the anode resistance increased from 133 to 304 Ω, resulting in the anode contributing 57% of the total internal resistance. The internal resistances of both electrodes observed here appear high because we use the absolute resistance, not area-based resistances. This high resistance is attributed to the fact that as the size of the reactor increases the absolute resistance must decrease. However, when the electrode area was taken into account to calculate the resistance, the electrode resistance of the C_1A_1 reactor was 20 mΩ m^2 (anode) and 35 mΩ m^2 (cathode), which are in a range of previously reported values of the anode resistance of MECs and MFCs (11–290 mΩ m^2) and cathode resistance of MECs (8–65 mΩ•m^2 for the cathode) of laboratory-sized reactors (Table S1). The cathodes of the MFCs were not considered in this comparison because of the different reaction in an MFC (oxygen reduction reaction) to that of the MEC (hydrogen evolution reactions). The solution resistances measured using EIS (Fig. S3) showed similar values (37–52 Ω) reflecting small changes in solution resistance due to slight differences in electrode distances or the relative sizes of the electrodes for the different S_R conditions in the MECs.

The relative importance of the anode to the total internal resistance in MECs has varied based on the different reactor configurations, materials, and operational conditions such as E_{ap}. For example, in a two-chamber MEC with a felt anode and Pt-catalyzed cathode, the anode pressed up against a anion exchange membrane was calculated to be the largest component of the internal resistance (59%) [14]. In an MEC using plain carbon cloth as both anodes and cathodes, the anode had a 2.7–3.2-fold higher resistance than the cathode [34]. In other MEC studies, however, where the anode was a high surface area graphite brush, the anode contributed only 19–27% of the total internal resistance [35]. The lower resistance of brush anodes compared to cathodes for the oxygen reduction reaction has also been found for MFCs [10]. In the MECs

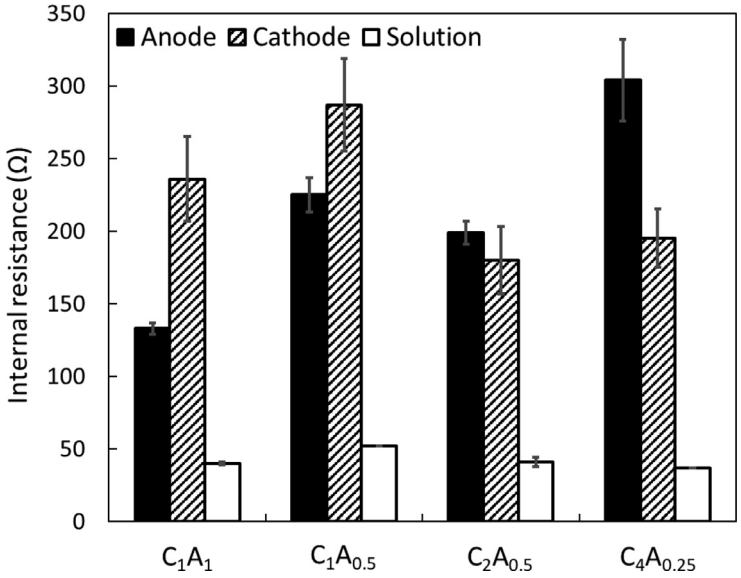

Fig. 4. Distribution of individual components of the internal resistance depending on the relative electrode surface area ratios. The resistances for the anode and cathode were calculated using the EPS method, and solution resistance was calculated using EIS data.

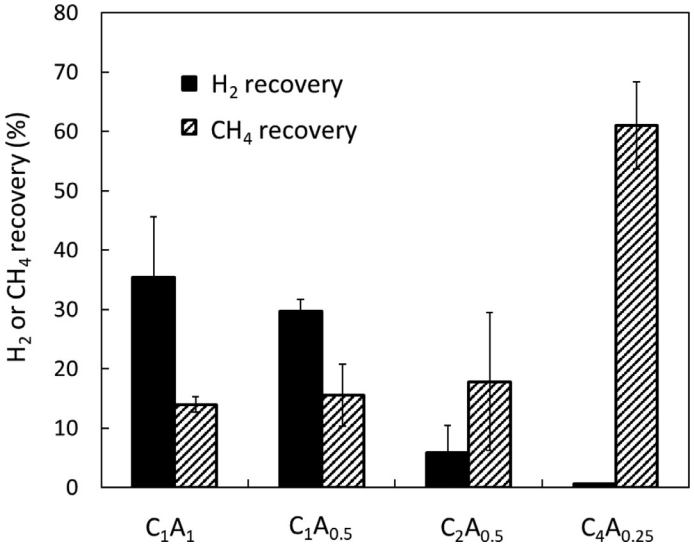

Fig. 5. Hydrogen and methane recovery efficiencies for the different electrode surface area ratios.

tested here, the relative contribution of the anode to the total internal resistance increased as the anode became smaller. By using equally sized electrodes it was possible to avoid a limiting current as well as reduce the impact of the anode on internal resistance and thus current generation.

3.4. Biogas production and organic removal

The electrode size ratio affected not only the limiting current but also the composition and volume of the biogas produced. H_2 was primarily recovered from MECs with lower S_R values, and higher concentrations of CH_4 in the biogas produced at the higher S_R values (Fig. 5). Also, the sum of cathodic H_2 and CH_4 recovery (γ_{CAT}) decreased inversely with S_R for three of the MECs, with γ_{CAT} = 49 ± 9% (S_R=1, C_1A_1), 45 ± 5% (S_R=2, $C_1A_{0.5}$), and 24 ± 14% (S_R=4, $C_2A_{0.5}$). The MEC with the highest S_R =16 ($C_4A_{0.25}$), however, produced mostly CH_4 gas with γ_{CAT} of 62 ± 7%. The lower cathodic biogas recoveries indicated a greater loss of the electrons produced by the anode that were not recovered as biogas, for example owing to the H_2 consumption by other scavenging routes [36,37].

The coulombic efficiency showed large changes with the electrode size ratio. At lower S_R values (1, 2 and 4), H_2 gas cycling seemed to occur on the anode. For three of these MECs the coulombic efficiency was much higher than 100%, with CE's of 165 ± 27% (S_R =1, C_1A_1), 163 ± 16% (S_R=2, $C_1A_{0.5}$), and 250 ± 93% (S_R=4, $C_2A_{0.5}$). In addition, they also had relatively lower COD removal efficiencies (64–80%) compared to the MEC with the largest S_R =16 configuration ($C_4A_{0.25}$) which had a COD removal of 87% (Fig. 6). In addition, there was a lower but appreciable amount of current produced late in the cycle for the lower S_R MECs which combined with the high CEs suggested H_2 gas cycling (Fig. 2A). To confirm the importance of H_2 cycling, N_2 gas was continuously sparged to the medium during one cycle using the $C_2A_{0.5}$ MEC which had the highest CE value. When this MEC was sparged with N_2 the current dropped rapidly to ~18 A m^{-3} after it reached the maximum, which was much lower value than the current produced without N_2 sparging (~220 A m^{-3}) (Fig. S4). With continuous N_2 sparging the coulombic efficiency decreased to less than 100% (CE = 96%) and the COD removal increased to 94%. Thus, hydrogen cycling was concluded to sustain increased levels of current generation at the end of a cycle for the three MECs (S_R =1, 2 and 4).

Evidence for extensive hydrogenotrophic methanogenesis in the S_R=16 reactors ($C_4A_{0.25}$), in addition to H_2 cycling, was shown by its much lower CE of 105%. For this MEC there was also a high conversion rate of H_2 to methane, with a cathodic CH_4 recovery of 61 ± 7% and cathodic H_2 recovery of 0.6 ± 0.2% (Fig. 5), as previously observed in other MEC studies [38-40]. Higher CH_4 production in the $C_4A_{0.25}$ MEC was likely due to the small anode size which was already producing current at the maximum rate. The low H_2 partial pressure would have helped to maintain stable H_2-consuming activity of hydrogenotrophic methanogens [41]. The relatively low cathodic recoveries suggest that some H_2 cycling was still occurring despite the predominance of methane in this MEC.

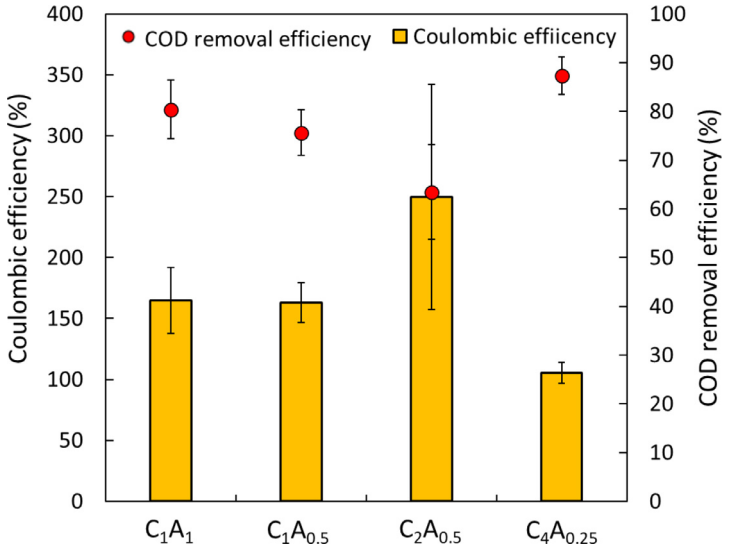

Fig. 6. Coulombic efficiencies and COD removals for the different electrode surface area ratios.

3.5. Implications for MEC operation

Polarization data obtained by varying E_{ap} have only infrequently been reported in MEC studies, but as shown here polarization curves can produce valuable insight into the performance of the system relative to energy efficiency. The few studies that have reported polarization data were useful in showing whether the anodes or cathodes were in a certain range for the desired reactions of organic oxidation at the anode and H_2 production at the cathode [42,43]. However, we further showed here that polarization data are a useful tool to estimate the maximum E_{ap} for different MEC configurations that will increase current and maximize energy recovery. For example, the energy efficiency here for the $C_4A_{0.25}$ was 79% for an applied voltage of E_{ap} = 0.9 V, which was a voltage that did not result in an increased current density compared to 0.7 V. Assuming the same amount of biogas was produced at E_{ap} = 0.7 V and 0.9 V, the energy efficiency would have been 102% ($C_4A_{0.25}$). This example shows that ~20% of input electrical energy could have been saved by using a lower E_{ap} of 0.7 V. Similarly, a rapid drop in H_2 production rate with sudden rise in the anode potential has been observed at E_{ap} beyond 0.7 V in a previous MEC study when highly conductive medium (20 mS/cm) was used [16]. The electrical efficiency was reduced from 241% (at 0.6 V) to 212% (at 0.7 V), suggesting that the energy efficiency could be improved by 14% by choosing an E_{ap} of 0.6 V rather than 0.7 V. Because I_{Lim} will likely vary for different MEC configurations, as it did here, it is recommended that polarization curves be routinely reported in MEC studies.

The method to identify maximum useful applied voltages here for MECs could also be used in studies where electrodes are inserted into tanks used for anaerobic digestion (AD), forming an AD-MEC [1]. In most of AD-MEC studies, only one or two E_{ap}'s have been used in the study and therefore there are no available polarization data to study the energy efficiency relative to the chosen applied potential. In addition, some very high E_{ap} have been used (> 1.0 V) with the goal of producing a high current density [44-46]. As we observed here, the optimal E_{ap} of the MECs really depends on the system configuration, thus choosing E_{ap} without any criteria based on polarization data could waste energy by selecting E_{ap} greater than those needed to achieve a high current. Also, the use of very high applied voltages could negatively impact current production by the bioanodes [47]. Thus, investigating and reporting polarization tests could be a method to better define an optimal value for E_{ap}. By monitoring the electrode potentials, the EPS method could also be used to determine the contributions of the individual electrodes and the solution to the total internal resistance. Such information could help to improve energy recovery through modifications to the components that are primarily limiting overall performance.

One concern for the study conditions could be that the small liquid volume might not translate to larger-scale systems. However, the performance of both large and small MECs are fundamentally limited by the internal resistance components. Thus, the methods used here to study a small configuration will provide the same information for larger reactors. For example, the EPS method used here has been tested on MFCs ranging from 28 mL reactors to 85 L reactors [10,48,49]. While the magnitude of the resistances may change for larger systems, the use of this method to examine the impact of changing the applied current will not be affected by the size the reactors. Small reactors such as those used here are appropriate for conducting high throughput bioelectrochemical studies as we can use many replicates and tests conditions, and the reactors have a very desirable high electrode packing density to improve MEC efficiencies. To provide information for more practical applications, further studies with larger scale reactors and continuous-flow operation will be needed, although the per-reactor costs of making larger reactors will likely limit the ability to run triplicate reactors as done here.

4. Conclusions

The impact of E_{ap} on MECs with different electrode size ratios was investigated using polarization tests. As the E_{ap} increased to the highest values (0.3 to 0.9 V) in several cases there was no corresponding increase in current at the higher E_{ap}'s. The I_{Lim} was measured for E_{ap} > 0.7 V of 5.1 A m^{-2} (S_R=16) or 3.9 A m^{-2} (S_R=4), suggesting that an E_{ap} above 0.7 V was not needed as using higher potentials would waste energy and not produce higher currents. The anode resistance was determined to be larger than cathode resistance for higher S_R values, which showed that the anodes were a major contributor to resistances that would reduce current production. The presentation of polarization data based on varying E_{ap} will therefore be a useful method to minimize wasting energy and better optimize electrical efficiency of MEC operation.

Author credit statement

B.E.L. and G.B. conceived the idea, G.B. collected and provided data curation, B.E.L. provided project administration, and G.B., R.R., and B.E.L. analyzed and interpreted the data, discussed the results, and contributed to writing, reviewing, and editing the final manuscript.

Supplementary information

mmc1.docx

Declaration of Competing Interest

The authors declare that they have no known competing financial interests or personal relationships that could have appeared to influence the work reported in this paper.

Acknowledgements

This project was funded by Penn State University and the Stan and Flora Kappe endowment.

References

[1] Z. Yu, X. Leng, S. Zhao, J. Ji, T. Zhou, A. Khan, A. Kakde, P. Liu, X. Li, A review on the applications of microbial electrolysis cells in anaerobic digestion, Bioresour. Technol. 255 (2018) 340–348.
[2] R.A. Rozendal, H.V. Hamelers, K. Rabaey, J. Keller, C.J. Buisman, Towards practical implementation of bioelectrochemical wastewater treatment, Trends Biotechnol. 26 (2008) 450–459.
[3] B.E. Logan, D. Call, S. Cheng, H.V. Hamelers, T.H. Sleutels, A.W. Jeremiasse, R.A. Rozendal, Microbial electrolysis cells for high yield hydrogen gas production from organic matter, Environ. Sci. Technol. 42 (2008) 8630–8640.
[4] W. Wang, B. Zhang, Z. He, Bioelectrochemical deposition of palladium nanoparticles as catalysts by Shewanella oneidensis MR-1 towards enhanced hydrogen production in microbial electrolysis cells, Electrochim. Acta 318 (2019) 794–800.
[5] R. Pinto, B. Tartakovsky, B. Srinivasan, Optimizing energy productivity of microbial electrochemical cells, J. Process Control 22 (2012) 1079–1086.
[6] D.C. Aiken, T.P. Curtis, E.S. Heidrich, Avenues to the financial viability of microbial electrolysis cells [MEC] for domestic wastewater treatment and hydrogen production, Int. J. Hydrogen Energy 44 (2019) 2426–2434.
[7] I. Ivanov, L. Ren, M. Siegert, B.E. Logan, A quantitative method to evaluate microbial electrolysis cell effectiveness for energy recovery and wastewater treatment, Int. J. Hydrogen Energy 38 (2013) 13135–13142.
[8] H. Guo, Y. Kim, Scalable multi-electrode microbial electrolysis cells for high electric current and rapid organic removal, J. Power Sources 391 (2018) 67–72.
[9] L. Lu, Z.J. Ren, Microbial electrolysis cells for waste biorefinery: A state of the art review, Bioresour. Technol. 215 (2016) 254–264.
[10] R. Rossi, B.P. Cario, C. Santoro, W. Yang, P.E. Saikaly, B.E. Logan, Evaluation of electrode and solution area-based resistances enables quantitative comparisons of factors impacting microbial fuel cell performance, Environ. Sci. Technol. 53 (2019) 3977–3986.
[11] Y. Fan, E. Sharbrough, H. Liu, Quantification of the internal resistance distribution of microbial fuel cells, Environ. Sci. Technol. 42 (2008) 8101–8107.
[12] V.J. Watson, B.E. Logan, Analysis of polarization methods for elimination of power overshoot in microbial fuel cells, Electrochem. Commun. 13 (2011) 54–56.
[13] H. Boghani, J.R. Kim, R.M. Dinsdale, A.J. Guwy, G.C. Premier, Reducing the burden of food processing washdown wastewaters using microbial fuel cells, Biochem. Eng. J. 117 (2017) 210–217.
[14] B.P. Cario, R. Rossi, K.-Y. Kim, B.E. Logan, Applying the electrode potential slope method as a tool to quantitatively evaluate the performance of individual microbial electrolysis cell components, Bioresour. Technol. 287 (2019) 121418.
[15] H. Liu, S. Grot, B.E. Logan, Electrochemically assisted microbial production of hydrogen from acetate, Environ. Sci. Technol. 39 (2005) 4317–4320.
[16] D. Call, B.E. Logan, Hydrogen production in a single chamber microbial electrolysis cell lacking a membrane, Environ. Sci. Technol. 42 (2008) 3401–3406.
[17] A. Thygesen, M. Marzorati, N. Boon, A.B. Thomsen, W. Verstraete, Upgrading of straw hydrolysate for production of hydrogen and phenols in a microbial electrolysis cell (MEC), Appl. Microbiol. Biotechnol. 89 (2011) 855–865.
[18] Y. Ruiz, J.A. Baeza, A. Guisasola, Microbial electrolysis cell performance using non-buffered and low conductivity wastewaters, Chem. Eng. J. 289 (2016) 341–348.
[19] R. Rossi, D.M. Hall, X. Wang, J.M. Regan, B.E. Logan, Quantifying the factors limiting performance and rates in microbial fuel cells using the electrode potential slope analysis combined with electrical impedance spectroscopy, Electrochim. Acta (2020) 136330.
[20] K. Guo, A. Prévoteau, K. Rabaey, A novel tubular microbial electrolysis cell for high rate hydrogen production, J. Power Sources 356 (2017) 484–490.
[21] H. Hu, Y. Fan, H. Liu, Hydrogen production using single-chamber membrane-free microbial electrolysis cells, Water Res. 42 (2008) 4172–4178.
[22] S. Cheng, B.E. Logan, High hydrogen production rate of microbial electrolysis cell (MEC) with reduced electrode spacing, Bioresour. Technol. 102 (2011) 3571–3574.
[23] F. Zhang, J. Liu, I. Ivanov, M.C. Hatzell, W. Yang, Y. Ahn, B.E. Logan, Reference and counter electrode positions affect electrochemical characterization of bioanodes in different bioelectrochemical systems, Biotechnol. Bioeng. 111 (2014) 1931–1939.
[24] B.E. Logan, E. Zikmund, W. Yang, R. Rossi, K.-Y. Kim, P.E. Saikaly, F. Zhang, Impact of ohmic resistance on measured electrode potentials and maximum power production in microbial fuel cells, Environ. Sci. Technol. 52 (2018) 8977–8985.
[25] S. Cheng, B.E. Logan, Increasing power generation for scaling up single-chamber air cathode microbial fuel cells, Bioresour. Technol. 102 (2011) 4468–4473.
[26] W. Yang, B.E. Logan, Immobilization of a metal–nitrogen–carbon catalyst on activated carbon with enhanced cathode performance in microbial fuel cells, ChemSusChem 9 (2016) 2226–2232.
[27] B.E. Logan, B. Hamelers, R. Rozendal, U. Schröder, J. Keller, S. Freguia, P. Aelterman, W. Verstraete, K. Rabaey, Microbial fuel cells: methodology and technology, Environ. Sci. Technol. 40 (2006) 5181–5192.
[28] K. Lawson, R. Rossi, J.M. Regan, B.E. Logan, Impact of cathodic electron acceptor on microbial fuel cell internal resistance, Bioresour. Technol. (2020) 123919.
[29] C.I. Torres, A. Kato Marcus, B.E. Rittmann, Proton transport inside the biofilm limits electrical current generation by anode-respiring bacteria, Biotechnol. Bioeng. 100 (2008) 872–881.
[30] P.-C. Nien, C.-Y. Lee, K.-C. Ho, S.S. Adav, L. Liu, A. Wang, N. Ren, D.-J. Lee, Power overshoot in two-chambered microbial fuel cell (MFC), Bioresour. Technol. 102 (2011) 4742–4746.
[31] J. Winfield, I. Ieropoulos, J. Greenman, J. Dennis, The overshoot phenomenon as a function of internal resistance in microbial fuel cells, Bioelectrochemistry 81 (2011) 22–27.
[32] X. Zhu, J.C. Tokash, Y. Hong, B.E. Logan, Controlling the occurrence of power overshoot by adapting microbial fuel cells to high anode potentials, Bioelectrochemistry 90 (2013) 30–35.
[33] Y. Hong, D.F. Call, C.M. Werner, B.E. Logan, Adaptation to high current using low external resistances eliminates power overshoot in microbial fuel cells, Biosens. Bioelectron. 28 (2011) 71–76.
[34] A. Miller, L. Singh, L. Wang, H. Liu, Linking internal resistance with design and operation decisions in microbial electrolysis cells, Environ. Int. 126 (2019) 611–618.
[35] X. Wang, R. Rossi, Z. Yan, W. Yang, M.A. Hickner, T.E. Mallouk, B.E. Logan, Balancing water dissociation and current densities to enable sustainable hydrogen production with bipolar membranes in microbial electrolysis cells, Environ. Sci. Technol. 53 (2019) 14761–14768.
[36] E. Lalaurette, S. Thammannagowda, A. Mohagheghi, P.-C. Maness, B.E. Logan, Hydrogen production from cellulose in a two-stage process combining fermentation and electrohydrogenesis, Int. J. Hydrogen Energy 34 (2009) 6201–6210.
[37] L. Wang, L. Singh, H. Liu, Revealing the impact of hydrogen production-consumption loop against efficient hydrogen recovery in single chamber microbial electrolysis cells (MECs), Int. J. Hydrogen Energy 43 (2018) 13064–13071.
[38] L. Gil-Carrera, A. Escapa, P. Mehta, G. Santoyo, S. Guiot, A. Morán, B. Tartakovsky, Microbial electrolysis cell scale-up for combined wastewater treatment and hydrogen production, Bioresour. Technol. 130 (2013) 584–591.
[39] N. Montpart, L. Rago, J.A. Baeza, A. Guisasola, Hydrogen production in single chamber microbial electrolysis cells with different complex substrates, Water Res. 68 (2015) 601–615.
[40] X. Li, C. Zeng, Y. Lu, G. Liu, H. Luo, R. Zhang, Development of methanogens within cathodic biofilm in the single-chamber microbial electrolysis cell, Bioresour. Technol. 274 (2019) 403–409.
[41] G. Baek, J. Kim, J. Kim, C. Lee, Role and potential of direct interspecies electron transfer in anaerobic digestion, Energies 11 (2018) 107.
[42] A.W. Jeremiasse, H.V. Hamelers, C.J. Buisman, Microbial electrolysis cell with a microbial biocathode, Bioelectrochemistry 78 (2010) 39–43.
[43] S. Rozenfeld, H. Teller, M. Schechter, R. Farber, O. Krichevski, A. Schechter, R. Cahan, Exfoliated molybdenum di-sulfide (MoS2) electrode for hydrogen production in microbial electrolysis cell, Bioelectrochemistry 123 (2018) 201–210.
[44] A. Ding, Y. Yang, G. Sun, D. Wu, Impact of applied voltage on methane generation and microbial activities in an anaerobic microbial electrolysis cell (MEC), Chem. Eng. J. 283 (2016) 260–265.
[45] H. Lin, N. Williams, A. King, B. Hu, Electrochemical sulfide removal by low-cost electrode materials in anaerobic digestion, Chem. Eng. J. 297 (2016) 180–192.
[46] Y. Chen, B. Yu, C. Yin, C. Zhang, X. Dai, H. Yuan, N. Zhu, Biostimulation by direct voltage to enhance anaerobic digestion of waste activated sludge, RSC Adv. 6 (2016) 1581–1588.
[47] G. Baek, L. Shi, R. Rossi, B.E. Logan, The effect of high applied voltages on bioanodes of microbial electrolysis cells in the presence of chlorides, Chem. Eng. J. 405 (2021) 126742.
[48] R. Rossi, B.E. Logan, Unraveling the contributions of internal resistance components in two-chamber microbial fuel cells using the electrode potential slope analysis, Electrochim. Acta (2020) 136291.
[49] R. Rossi, D. Jones, J. Myung, E. Zikmund, W. Yang, Y.A. Gallego, D. Pant, P.J. Evans, M.A. Page, D.M. Cropek, Evaluating a multi-panel air cathode through electrochemical and biotic tests, Water Res. 148 (2019) 51–59.